

# Electric and magnetic dipole coupling in near-infrared split ring metamaterial arrays

Ivana Sersic,\* Martin Frimmer, and A. Femius Koenderink  
 Center for Nanophotonics, FOM Institute for Atomic and Molecular Physics (AMOLF),  
 Science Park 113, 1098 XG Amsterdam, The Netherlands  
 (Dated: Uploaded on arxiv, July 17 2009.)

We present experimental observations of strong electric and magnetic interactions between split ring resonators (SRRs) in metamaterials. We fabricated near-infrared ( $1.4 \mu\text{m}$ ) planar metamaterials with different inter-SRR spacings along different directions. Our transmission measurements show blueshifts and redshifts of the magnetic resonance, depending on SRR orientation relative to the lattice. The shifts agree well with a simple model with simultaneous magnetic and electric near-field dipole coupling. We also find large broadening of the resonance, accompanied by a decrease in effective cross section per SRR with increasing density. These effects result from superradiant scattering. Our data shed new light on Lorentz-Lorenz approaches to metamaterials.

Since the seminal work of Veselago [1] and Pendry [2], many experimentalists have started to pursue optical materials with negative permittivity  $\epsilon$  and permeability  $\mu$  [3]. The key motivation is the prospect of ‘transformation optics’, which allows arbitrary bending of electromagnetic fields, provided one has full control over  $\epsilon$  and  $\mu$ . Particularly exciting examples are perfect lenses, that allow perfect sub-diffraction focusing of light [2], and ‘cloaks’ in which light passes around an object without scattering [4]. Full control over  $\epsilon$  and  $\mu$  requires ‘metamaterials’ of artificial nano-scatterers with electric and magnetic response, arranged in sub-wavelength arrays. The archetypical building block is the split ring resonator (SRR) consisting of a single cut metal loop with an inductive response. In recent years the field of metamaterials has made tremendous progress in shifting the magnetic response from microwave to optical frequencies [5, 6, 7, 8]. An important conceptual question is whether the effective response captured by  $\epsilon$  and  $\mu$  is influenced by coupling between constituents. So far, the effective response of SRR arrays has been entirely attributed to single, uncoupled constituents [5, 6, 7]. Nonetheless, recent theory and experiments show that SRRs can couple when stacked vertically with very small separation [9, 10]. Controlled coupling between magnetic scatterers can furthermore be of great use also outside the scope of metamaterials, for instance for magnetic particle waveguides [9, 11, 12, 13], antennas [14], metamaterial lasers [15], chiral materials [16], and for grating optics in which diffractive and constituent resonances coincide [17].

In this Letter we present the first systematic measurements of strong constituent coupling in planar SRR metamaterial arrays. We fabricated and characterized SRR lattices with a magnetic response at  $\lambda = 1.4 \mu\text{m}$  [6, 7] in which we vary the spacing between SRRs along different lattice directions independently. We observe large redshifts and blueshifts in the transmission resonances depending on SRR orientation relative to the lattices, which allow us to identify different coupling mechanisms. We establish that in-plane electric-electric dipole coupling and out-of-plane magnetic-magnetic dipole coupling are strong competing interactions. We explain the shifts by a quasistatic electric and magnetic dipole coupling model [10], that enables us to determine the magnetic and electric polarizability of SRRs. Finally, we discuss the role

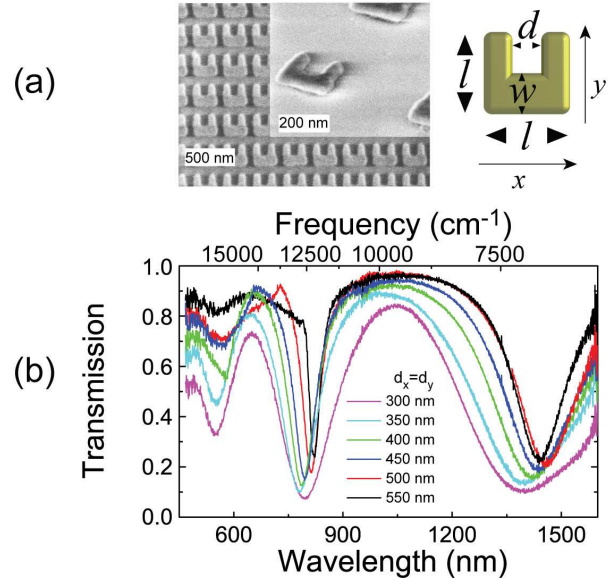


FIG. 1: (Color) (a) We fabricated arrays of Au SRRs on glass with periodicities  $d_{x,y} = 300 \text{ nm}$  (SEM micrograph) and larger (inset). Each SRR has  $l = 200 \text{ nm}$ ,  $w = 80 \text{ nm}$ , and SRR height  $30 \text{ nm}$  ( $\pm 5 \text{ nm}$ ). (b) Transmission spectra for square SRR arrays with split width  $d = 80 \text{ nm}$  (polarization along  $x$ ). The magnetic resonance at  $1.4 \mu\text{m}$  blue-shifts and broadens with increasing density.

of dynamic effects on the metamaterial response, which are evident in density-dependent resonance broadening and a saturation of the transmission resonance.

We have fabricated Au SRRs on glass substrates by electron beam lithography and lift-off using PMMA resist [13], without any adhesive layers. We took great care to produce SRRs of identical dimension in arrays of different densities, using digital image analysis of SEM micrographs (see Fig. 1(a)) to overcome proximity effects. Based on [6], our SRRs ( $200 \text{ nm}$  base) are expected to have an LC resonance (generally referred to as ‘magnetic’) at  $1.4 \mu\text{m}$ . To resolve the coupling strength between SRRs along the  $x$  (along SRR base) and  $y$  (along SRR arms) directions separately, we varied the pitches  $d_x$  and  $d_y$  independently between  $300 \text{ nm}$  and  $550 \text{ nm}$ , staying below  $550 \text{ nm}$  to avoid grating diffraction in the range of

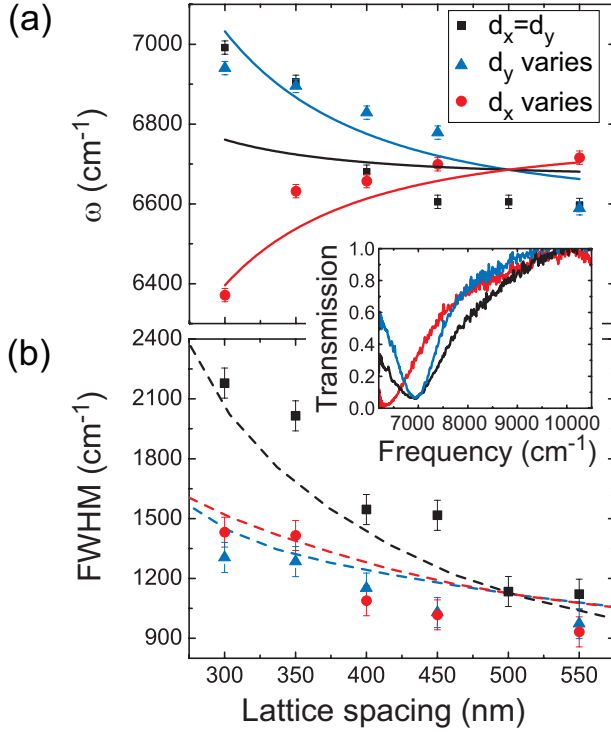


FIG. 2: (Color)(a) Frequency of the magnetic resonance versus lattice spacing. The frequency blue-shifts when decreasing  $d_y$  whether  $d_y = d_x$  (black squares) or not (blue circles,  $d_x = 500$  nm), while it red-shifts when decreasing  $d_x$  (red triangles,  $d_y = 500$  nm). The inset shows raw spectra for  $d_x = d_y = 300$  nm (black curve),  $d_x = 500$  nm,  $d_y = 300$  nm (blue curve),  $d_x = 300$  nm,  $d_y = 500$  nm (red curve). (b) FWHM of the magnetic resonance versus lattice spacing (color coding as in (a)). Curves are theory (electrostatic in (a), electrodynamic in (b)).

the magnetic resonance. We measured polarization-resolved normal incidence transmission using the set up reported in Ref. [13]. We illuminated a mm-sized area on the sample with a beam from a halogen lamp ( $5^\circ$  opening angle) and used a  $20 \mu\text{m}$  pinhole in an intermediate image plane to select the transmitted intensity from single  $36 \times 36 \mu\text{m}^2$  SRR arrays, which we spectrally resolved by cooled Si CCD and InGaAs array spectrometers, and normalized to transmitted intensity through bare substrate.

Fig. 1(b) shows transmission spectra measured on a sample with square lattices (various  $d_x = d_y$ ) of SRRs with split width  $d = 80$  nm. We observe the magnetic resonance at  $1.4 \mu\text{m}$  only for polarization along  $x$ , as reported by [6, 7, 18], as well as higher order plasmon resonances at  $500$  nm and  $800$  nm [6]. In the remainder of this Letter, we focus on the magnetic resonance. Tracing the resonance minimum in transmission versus SRR density in Fig. 1(b), we find that the resonance blue-shifts as SRRs are brought closer. A blueshift upon increased coupling is expected for transverse coupling of magnetic dipoles, in analogy to electric dipole coupling in plasmon systems [11, 12, 19]. Such transverse coupling is expected since the magnetic dipoles are all oriented perpen-

dicular to the SRR plane. To study this coupling in detail, we fabricated samples with a large set of SRR arrays (split width  $d = 100$  nm) where  $d_x$  and  $d_y$  are varied independently. We expect a blueshift with increasing density for all arrays since the magnetic dipoles are always transversely coupled. In Fig. 2(a) we plot the measured center frequency of the resonance versus SRR spacing for three sets of arrays. For the first set  $d_x = d_y$ , we indeed observe a continuous blue-shift, confirming the data for split width  $d = 80$  nm in Fig. 1(b). We also observe a blueshift for the second set when only  $d_y$  is varied ( $d_x = 500$  nm). Remarkably, we measure a redshift for the third case, when only  $d_x$  decreases and  $d_y$  is fixed at  $500$  nm. This result is surprising since red-shifts imply longitudinal coupling, which is inconsistent with the orientation of the magnetic dipoles. The redshift can only be understood by noting that SRRs also have an electric polarizability in addition to a magnetic dipole [10, 18]. The electric dipole moment points along the SRR base, hence allowing for longitudinal coupling of SRRs. We implement a model that takes into account simultaneous electric and magnetic dipole coupling, similar to the model for vertically stacked SRR dimers reported in [10]. In this model, all magnetic dipoles couple transversely while electric dipoles transversely couple along  $y$  and longitudinally along  $x$ . We limit ourselves to electrostatic and magnetostatic nearest-neighbor coupling, thereby ignoring electro-dynamic effects, the air-glass interface, and multipole corrections. However, this model captures the main physics embodied in our observations. The eigenfrequencies of the system can be determined from the Lagrangian

$$\mathcal{L} = \sum_{i,j} \left[ \frac{L}{2} (\dot{Q}_{i,j}^2 - \omega_0^2 Q_{i,j}^2) - \frac{M_h}{d_x^3} \dot{Q}_{i,j} \dot{Q}_{i+1,j} - \frac{M_h}{d_y^3} \dot{Q}_{i,j} \dot{Q}_{i,j+1} + 2 \frac{M_e \omega_0^2}{d_x^3} Q_{i,j} Q_{i+1,j} - \frac{M_e \omega_0^2}{d_y^3} Q_{i,j} Q_{i,j+1} \right], \quad (1)$$

where  $L$  is the SRR inductance,  $Q_{i,j} (\dot{Q}_{i,j})$  represents the charge (current) on the SRR at site  $(i, j)$ , and where  $M_h$  and  $M_e$  quantify the mutual inductance and the electric dipole coupling. Solving Eq. (1) for the resonance frequency at normal incidence ( $k_{\parallel} = 0$ ) yields

$$\omega = \omega_0 \sqrt{\frac{1 - \frac{4\kappa_e}{d_x^3} + \frac{2\kappa_e}{d_y^3}}{1 - \frac{2\kappa_h}{d_x^3} - \frac{2\kappa_h}{d_y^3}}} \quad (2)$$

where  $\omega_0$  is the resonance frequency of a single SRR, and where  $\kappa_e = M_e/L$  and  $\kappa_h = M_h/L$ . We fix  $\kappa_e = 1.04 \cdot 10^{-21} \text{ m}^3$  to match the SRR electric polarizability to the resonant extinction cross section of  $0.3 \mu\text{m}^2$  measured by Husnik *et al.* [20, 21]. Fig. 3(a) shows the resonance  $\omega$  versus  $d_{x,y}$  for the case of magnetic coupling only ( $\kappa_e = 0$ ). The resonance blue-shifts for decreasing  $d_{x,y}$  in all cases due to transverse magnetic dipole coupling. Fig. 3(b) shows the resonance frequency for electric coupling only ( $\kappa_h = 0$ ). The resonance red-shifts with increasing density unless  $d_x$  is fixed

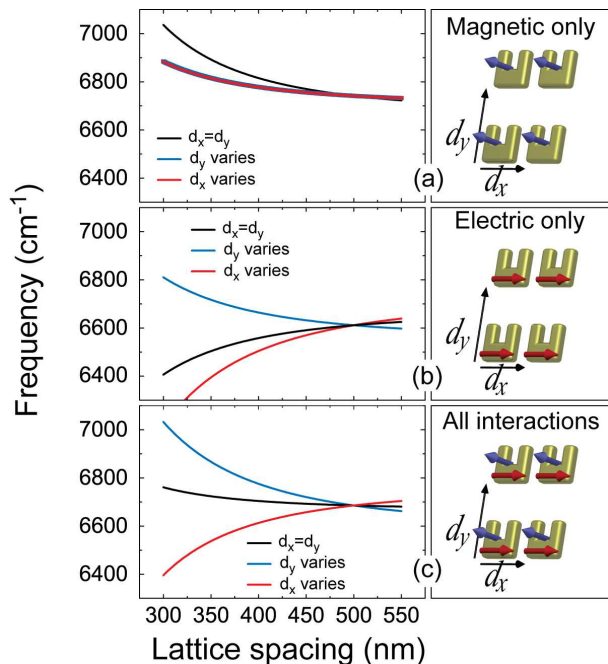


FIG. 3: (Color) Electrostatic calculation of the magnetic resonance frequency as a function of lattice spacing. Black curves:  $d_x = d_y$ . Blue curves:  $d_y$  varies at fixed  $d_x = 500$  nm. Red curves:  $d_x$  varies at fixed  $d_y = 500$  nm. For magnetic coupling only (a), resonances always blue-shift with decreasing lattice spacing, while for electric coupling only (b), the behavior of the resonances for  $d_x = d_y$  changes sign with respect to (c) (all couplings). Insets in (a), (b) and (c) are sketches of the electric and magnetic coupling between SRRs. Curves in (c) are reproduced in Fig. 2.

at 500 nm. This result indicates that longitudinal coupling exceeds transverse coupling in square lattices of strictly in-plane dipoles. Neither model with solely electric or solely magnetic interaction is consistent with our measurements, since we observe blue-shifts in all cases except when  $d_x$  is varied and  $d_y$  is fixed. Fig. 3(c) shows the calculated resonance  $\omega$  taking into account both electric and magnetic dipole interactions, assuming  $\kappa_e/\kappa_h = 1.5$ . As in the data, the resonance only red-shifts when decreasing the distance  $d_x$  at large  $d_y$ . In this case longitudinal electric coupling exceeds the sum of transverse electric and magnetic coupling, leading to a net redshift. For a quantitative comparison with our measurements we plot the shifts in Fig. 3(c) together with the data in Fig. 2. The good quantitative agreement, shows that the model, which has no adjustable parameters, confirms our interpretation that SRRs in metamaterial arrays show strong electric and magnetic dipole-dipole interactions. These interactions are best quantified in data on rectangular arrays, since the interactions in square arrays studied so far [6, 7] are obscured by partial cancellation of the electrically and the magnetically induced shift. In our comparison we used  $\kappa_e/\kappa_h = 1.5$  measured in [10] for vertically stacked SRRs. The data show that this ratio is also relevant for simultaneous electric and magnetic dipole coupling in the  $xy$ -plane, allowing a direct identification of  $\kappa_e$  and  $\kappa_h$  with

on-resonance electric and magnetic point polarizabilities (see note [21]).

A striking feature in our transmission data (*cf.* Fig. 1(b)) in addition to the spectral shifts, is the large broadening of the resonance as the density of SRRs increases. In Fig. 2(b) we plot the measured full width at half minimum (FWHM) of the transmission minimum versus lattice spacing. For square lattices, the width more than doubles from 1000 to 2150  $\text{cm}^{-1}$  as the pitch is reduced from 550 to 300 nm, while for both types of rectangular lattices ( $d_x$  or  $d_y$  fixed at 500 nm) the width increases from 950 to 1400  $\text{cm}^{-1}$ . Such broadening was also noted by Rockstuhl et al. [7] for square arrays. Our extensive data on many rectangular and square arrays allow us to quantitatively identify the source of broadening. From the outset it is clear that the broadening is outside the scope of our Lagrangian model, since the (Ohmic) damping rate of coupled oscillators remains almost unchanged in any electrostatic model. Instead, electrodynamical radiation damping must be taken into account. As all oscillators in our sub-diffraction lattices are driven in phase ( $k_{\parallel} = 0$ ), scattered light radiated by all oscillators interferes destructively for all angles, except along the transmitted and reflected direction. Since the magnetic dipoles are aligned along the incident beam, they do not radiate any amplitude into the  $k_{\parallel} = 0$  directions. Hence, all radiation damping is *solely* due to the induced *electric* dipoles. For a quantitative analysis we use an electrodynamic model for Lorentzian electric point dipoles [12, 17, 21] resonant at 1.4  $\mu\text{m}$  and with the material loss of Au. This model has no adjustable parameters, since the polarizability is fixed [21] to match the extinction cross section of single SRRs in [20]. The dynamical model quantitatively reproduces the measured broadening with decreasing pitch for all lattices (curves in Fig. 2(b)). An important conclusion is that the large width of the magnetic response commonly observed for SRR arrays [5, 6, 7] is not due to intrinsic loss, but is quantitatively consistent with superradiant decay of the electric dipoles. The collective enhancement of the single SRR radiative linewidth, already suspected by [7], implies enhanced scattering and a reduction of the absorption of the array far below the albedo of single SRRs.

Finally we correlate the resonance broadening with the measured transmission  $T$  on resonance. Fig. 4 shows the effective extinction cross section derived from our measurements through  $\sigma_{\text{eff}} = d_x d_y (1 - T)$ . For uncoupled scatterers (dilute samples) we expect constant  $\sigma_{\text{eff}}$  equal to the extinction cross section 0.3  $\mu\text{m}^2$  measured for a single SRR in [20] (dashed line in Fig. 4), as indeed almost found in our data for  $d_x = d_y > 500$  nm. We measure effective cross sections far below the true  $\sigma_{\text{ext}}$  for  $d < 500$  nm, indicative of strong dipole-dipole coupling. The collective superradiant decay (Fig. 2(b)) which widens the resonance also reduces the extinction cross section per element to remain below the unit-cell area  $d_x d_y$  (curves in Fig. 4).

In conclusion, we have measured large resonance shifts as a function of density in SRR arrays resonant at around  $\lambda = 1.4 \mu\text{m}$ . These shifts are due to strong near-field elec-



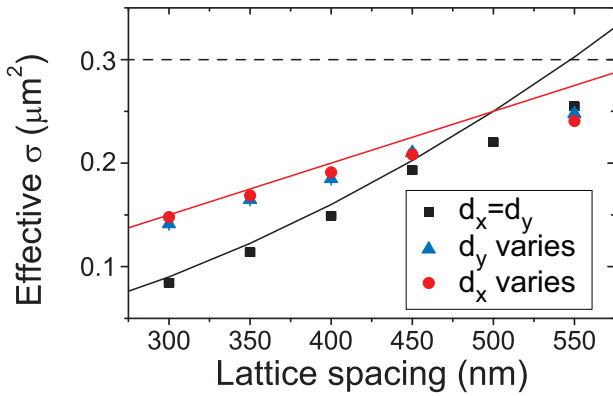


FIG. 4: Effective extinction cross section per SRR derived from on-resonance transmission. The black dashed line indicates the extinction cross section for a single SRR (from [20]). The effective extinction cross section decreases with increasing density, and is limited by the area  $d_x d_y$  of the unit cell (black and red lines).

trostatic and magnetostatic dipole coupling. Furthermore, we have observed electrodynamic superradiant damping that is evident in our data as a resonance broadening and as an effective reduction of the extinction cross section per SRR. Since the data show that the response of SRR arrays is not simply given by the product of the density and polarizability of single constituents, we conclude that a Lorentz-Lorenz analysis to explain effective media parameters of metamaterials ‘atomistically’ is not valid [22]. The fact that the Lorentz-Lorenz picture is invalid has important repercussions: It calls for a shift away from the paradigm that the highest polarizability per constituent is required to obtain the strongest magnetic response. Indeed, our experiments clearly show that increasing the density of constituents to raise the magnetic response [6] is ineffective, since superradiant damping limits the achievable response. To strengthen  $\mu$ , we propose that one ideally finds constituents that have both a smaller footprint *and a smaller polarizability* per constituent. We stress that even if constituent coupling modifies  $\epsilon$  and  $\mu$ , this does not call into question the effective media parameters per se. The effective medium regime only breaks down when constituent coupling is so strong that collective modes of differently shaped macroscopic objects carved from the same SRR array have very different resonance frequencies. In this regime interesting physics comes into view, particularly regarding active devices. Specific examples are array antennas for spontaneous emission [14] and ‘lasing spasers’ [15], where the lowest-loss array mode will lase most easily.

We thank Chris Rétif for assistance with sample fabrication and Ewold Verhagen, Dries van Oosten, Jaime Gómez Rivas, Albert Polman and Kobus Kuipers for assistance with equipment and stimulating discussions. This work is part of the research program of the “Stichting voor Fundamenteel Onderzoek der Materie (FOM),” which is financially supported by the “Nederlandse Organisatie voor Wetenschappelijk Onderzoek (NWO).”

\* Electronic address: i.sersic@amolf.nl;

URL: <http://www.amolf.nl/research/resonant-nanophoto>

- [1] V. G. Veselago, *Sov.Phys. USPEKHI* **10**, 509-514 (1968).
- [2] J. B. Pendry, *Phys. Rev. Lett.* **85**, 3966 (2000).
- [3] J. B. Pendry, *Physics World* **14**, 47 (2001); C. M. Soukoulis, S. Linden, and M. Wegener, *Science* **315**, 47 (2007); V. M. Shalaev, *Nature Photonics* **1**, 41 (2007).
- [4] U. Leonhardt, *Science* **312**, 1777 (2006); J. B. Pendry, D. Schurig, and D. R. Smith, *ibid.*, 1780 (2006).
- [5] D. R. Smith, W. J. Padilla, D. C. Vier, S. C. Nemat-Nasser, and S. Schultz, *Phys. Rev. Lett.* **84**, 4184 (2000); W. J. Padilla, A. J. Taylor, C. Highstrete, M. Lee, and R. D. Averitt, *ibid.* **96**, 107401 (2006); S. Linden, C. Enkrich, M. Wegener, J. Zhou, T. Koschny, and C. M. Soukoulis, *Science* **306**, 1351 (2004).
- [6] C. Enkrich, M. Wegener, S. Linden, S. Burger, L. Zschiedrich, F. Schmidt, J. F. Zhou, T. Koschny, and C. M. Soukoulis, *Phys. Rev. Lett.* **95**, 203901 (2005).
- [7] C. Rockstuhl, T. Zentgraf, H. Guo, N. Liu, C. Etrich, I. Loa, K. Syassen, J. Kuhl, F. Lederer, and H. Giessen, *Appl. Phys. B* **84**, 219 (2006).
- [8] A. N. Grigorenko, A. K. Geim, H. F. Gleeson, Y. Zhang, A. A. Firsov, I. Y. Khrushchev, and J. Petrovic, *Nature* **438**, 335 (2005); V. M. Shalaev, W. Cai, U. K. Chettiar, H.-K. Yuan, A. K. Sarychev, V. P. Drachev, and A. V. Kildishev, *Opt. Lett.* **30**, 3356 (2005); G. Dolling, M. Wegener, C. M. Soukoulis, and S. Linden, *Opt. Lett.* **32**, 53 (2007).
- [9] E. Shamonina, V. A. Kalinin, K. H. Ringhofer, and L. Solymar, *J. Appl. Phys.* **92**, 6252 (2002).
- [10] N. Liu, H. Liu, S. N. Zhu, and H. Giessen, *Nature Photonics* **3**, 157 (2009).
- [11] M. L. Brongersma, J. W. Hartman, and H. A. Atwater, *Phys. Rev. B* **62**, R16356 (2000).
- [12] A. F. Koenderink and A. Polman, *Phys. Rev. B* **74**, 033402 (2006).
- [13] A. F. Koenderink, R. de Waele, J. C. Prangsma, and A. Polman, *Phys. Rev. B* **76**, 201403R (2007).
- [14] J. Li and N. Engheta, *Phys. Rev. B* **74**, 115125 (2006).
- [15] N. I. Zheludev, S. L. Prosvirnin, N. Papisimakis, and V. A. Fedotov, *Nature Photonics* **2**, 351 (2008).
- [16] S. Zhang, Y.-S. Park, J. Li, X. Lu, W. Zhang, and X. Zhang, *Phys. Rev. Lett.* **102**, 023901 (2009); E. Plum, J. Zhou, J. Dong, V. A. Fedotov, T. Koschny, C. M. Soukoulis, N. I. Zheludev, *Phys. Rev. B* **79**, 035407 (2009); M. Wegener and S. Linden, *Physics* **2**, 3 (2009).
- [17] F. J. García de Abajo, *Rev. Mod. Phys.* **79**, 1267 (2007).
- [18] N. Katsarakis, T. Koschny, M. Kafesaki, E. N. Economou, and C. M. Soukoulis, *Appl. Phys. Lett.* **84**, 2943 (2004).
- [19] E. Prodan, C. Radloff, N. J. Halas, and P. Nordlander, *Science* **302**, 419 (2003); P. Nordlander, C. Oubre, E. Prodan, K. Li, and M. I. Stockman, *Nano Lett.* **4**, 899 (2004).
- [20] M. Husnik, M. W. Klein, N. Feth, M. König, J. Niegemann, K. Busch, S. Linden and M. Wegener, *Nature Photonics* **2**, 614 (2008).
- [21] We use  $\sigma_{\text{ext}} = 4\pi k \text{Im}\alpha$  with  $k = 2\pi/\lambda$ , using the Lorentzian electric polarizability  $\alpha_0 = \omega_0^2 \kappa_e / (\omega_0^2 - \omega^2 - i\omega\gamma)$  implicit in Eq. (2), and with radiation damping  $1/\alpha = 1/\alpha_0 - i\frac{2}{3}k^3$  [12]. We take  $\gamma = 1.2 \cdot 10^{14} \text{ s}^{-1}$  for the Ohmic damping of Au from P. B. Johnson and R. W. Christy, *Phys. Rev. B.* **6**, 4370 (1972).
- [22] C. R. Simovski and S. A. Tretyakov, *Phys. Rev. B* **75**, 195111 (2007).